Chapter 4
A Few Other Interesting Chaotic Delay Differential Equations

4.1 Introduction

One of the well known properties of DDEs is that their effective dimensions increase with the delay time τ [1, 2], see Sect. 1.2.2. This allows one to select different values (sufficiently large) for the delay time τ to generate high-dimensional chaotic signals. Hence, in recent times DDEs have received increased attention in the nonlinear dynamics literature due to the possibility of generating more complex and high-dimensional chaotic attractors and also because of the feasibility of their experimental realization. Therefore, several chaotic time-delay systems and their variants have been proposed during the past few years for generating and enhancing complexity of chaotic behavior in various technological and engineering applications. In this chapter, we will briefly review the dynamical properties of some of the most important first order scalar nonlinear time-delay systems, that have been widely used in the literature, exhibiting chaotic/hyperchaotic behaviors. In addition, we will also present some of the interesting coupled (higher order) delay differential equations in different areas of science and technology.

4.2 The Mackey-Glass System: A Typical Nonlinear DDE

In order to gain further insight and clear understanding of the general features of the dynamics of nonlinear DDEs, in this section, we will consider another scalar first order nonlinear DDE, namely the Mackey-Glass equation, which has been well studied in the literature in connection with chaotic dynamics and applications. As noted in the previous chapter, it is quite intricate to obtain even the stability criteria for the fixed point solution of a scalar nonlinear DDE itself. Now we will consider the Mackey-Glass system as another example to discuss the dynamics of nonlinear DDEs. Other examples are discussed in the following sections.

4.2.1 Mackey-Glass Time-Delay System

The Mackey-Glass time-delay system [3, 4] has been a well studied nonlinear DDE equation in the literature for its chaotic dynamics [1, 5–10]. It has received a central

M. Lakshmanan, D.V. Senthilkumar, *Dynamics of Nonlinear Time-Delay Systems*,
Springer Series in Synergetics, DOI 10.1007/978-3-642-14938-2_4,

importance in recent studies on synchronization in view of its hyperchaotic behavior [11–16]. Analog version of the Mackey-Glass system has also been realized experimentally using electronic circuits [14–17]. The Mackey-Glass system, which was originally deduced as a model for blood production in patients with leukemia, can be represented by the first order nonlinear DDE

$$\dot{x} = -bx(t) + \frac{ax(t-\tau)}{(1.0 + x(t-\tau)^c)}, \tag{4.1}$$

where a, b and c are positive constants. Here, $x(t)$ represents the concentration of blood at time t (density of mature cells in bloodstreams), when it is produced, $x(t-\tau)$ is the concentration when the "request" for more blood is made and τ is the time-delay between the production of immature cells in the bone marrow and their maturation for release in circulating bloodstreams. In patients with leukemia, the time τ may become excessively large, and the concentration of blood will oscillate, or if τ is even larger, the concentration can vary chaotically, as demonstrated by Mackey and Glass [1, 3]. This model is often used as a prototype model in the literature for nonlinear delay systems exhibiting chaotic attractors and even hyperchaotic attractors for large values of delay time.

4.2.2 Fixed Points and Linear Stability Analysis

A great deal of information can be obtained about the dynamical behavior of the scalar first order Mackey-Glass DDE (4.1) by performing a linear stability analysis [18] of equilibrium states. As pointed out in Chap. 3, the difficulty lies in obtaining the conditions under which the real part of the eigenvalues of the linearized equation for the given fixed point is less than zero from the resulting transcendental characteristic equation.

The steady state or equilibrium state (fixed point) of the system (4.1) is one for which $x(t) = x(t-\tau) = x(0) = x^* \; \forall \, t$ and as a consequence all the time derivatives vanish identically. Hence substituting $x(t) = x(t-\tau)$ and $\dot{x} = 0$ in (4.1), it is easy to see that Eq. (4.1) has two fixed points,

$$x = x^* = 0, \tag{4.2a}$$

$$x = x^* = \left(\frac{a-b}{b}\right)^{\frac{1}{c}}. \tag{4.2b}$$

Note that the second solution exists only for $a > b$ (x is real). The stability of the fixed points is determined by examining how a small perturbation about the fixed point behaves in time for all $t > 0$. In particular, as pointed out in Chap. 3, Sect. 3.2.1, to study the linear stability we assume that the perturbations about the fixed point grows as $\rho \exp \lambda t$, where λ is in general a complex number to be determined and $\rho \ll 1$ is the amplitude of the perturbation, Then the characteristic equation turns out to be

$$\lambda = -b + \left(\frac{a(1+x^*) - acx^*}{(1+x^*)^2} \right) \exp(-\lambda\tau). \tag{4.3}$$

Solving the above equation for λ for either of the fixed points $x^* = 0$ or $x^* = \left(\frac{a-b}{b}\right)^{\frac{1}{c}}$ gives the criterion for the stability of the corresponding fixed points. In the following we analyze the stability of the above two fixed points given by Eqs. (4.2) both in the absence and presence of time-delay τ.

4.2.3 Time-Delay $\tau = 0$

Now, we will discuss the stability of the fixed points (4.2) in the absence of time-delay, that is $\tau = 0$.

(a) Fixed point $x^* = 0$:
From Eq. (4.3), one finds the characteristic equation for the fixed point $x = x^* = 0$ to be

$$\lambda + b - a = 0, \tag{4.4}$$

and the fixed point is stable for $a < b$.

(b) Fixed point $x^* = \left(\frac{a-b}{b}\right)^{\frac{1}{c}}$:

The characteristic equation for the second fixed point $x = x^* = \left(\frac{a-b}{b}\right)^{\frac{1}{c}}$ can be written as

$$\lambda + b - b(1 - ac + bc) = 0, \tag{4.5}$$

and the fixed point is stable if $a > b$.

Thus for $a < b$ we have $x = x^* = 0$ as the only locally stable fixed point. For $a > b$ the second fixed point, $x^* = \left(\frac{a-b}{b}\right)^{\frac{1}{c}}$, is created while the first one, $x^* = 0$, becomes unstable. Obviously $a = b$ is a bifurcation point.

4.2.4 Time-Delay $\tau > 0$

In this section, we will make use of the approach advocated in Chaps. 2 and 3 in order to (i) determine the parametric conditions due to which change in the stability of a given fixed point occurs as specified by the transcendental equation, (ii) to demarcate the asymptotically stable regions of the fixed points in the parameter space of the system and (iii) to determine the conditions on the parameters under which the given fixed point of the system is stable.

4.2.4.1 Geometric Approach

Now let us apply the geometric approach proposed by McDonald [19] to determine the stability from the general equation (4.3) as discussed in Sect. 2.3 of Chap. 2. As pointed out earlier, a change in stability of a fixed point can occur only when a root $\lambda = \alpha + i\beta$ of Eq. (4.3) crosses the imaginary axis, that is, $\lambda = i\beta$, where β is real, is a solution of Eq. (4.3). In particular let us consider the transcendental equation

$$\lambda + b - ae^{-\lambda\tau} = 0, \tag{4.6}$$

corresponding to the fixed $x^* = 0$ for $\tau > 0$. Now, if a substitution $\lambda = i\beta$ is made in the above equation, then it takes the following form

$$\frac{b + i\beta}{a} = \exp(-i\beta\tau). \tag{4.7}$$

If the steady state in question is stable in the absence of delay, that is for $\tau = 0$, an instability can occur for $\tau \neq 0$ only if there are some real β and τ for which the Eq. (4.7) holds good. This can be determined by the simple geometric construction discussed in Sect. 2.3 of Chap. 2.

Considering the right hand side of Eq. (4.7), we can easily see that it traces a unit circle as shown in Fig. 4.1 and change in stability of the fixed point is indicated by the intersection of the ratio curve, namely the left hand side of Eq. (4.7). This is examined by changing the value of a in the Eq. (4.6), whose value determines the stability of the fixed point $x^* = 0$. As a typical example, for the values of the parameters $\tau = 25.0$, $b = 0.1$ and $a = 0.09$, it turns out that $a < b$ and the ratio curve (dotted line) does not intersect the unit circle as shown in the Fig. 4.1a. Thus the fixed point $x^* = 0$ remains stable. As the value of a is increased to $a = 0.1$ so that $a = b$, one finds the ratio curve (dotted line) just touches the unit circle (Fig. 4.1b) indicating the boundary layer between the stability of the two fixed points. For $a = 0.11$, when $a > b$, the ratio curve intersects the unit circle as shown in Fig. 4.1c indicating the change in stability of the first fixed point $x^* = 0$, which becomes unstable for the latter value of a.

Similarly, using the above geometric construction, one can also determine the stability of the second fixed point $x^* = \left(\frac{a-b}{b}\right)^{\frac{1}{c}}$ from its characteristic (transcendental) equation

$$\lambda + b - b(1 - ac + bc)e^{-\lambda\tau} = 0, \tau > 0. \tag{4.8}$$

Again substituting $\lambda = i\beta$ and rewriting the above transcendental equation in the form of Eq. (4.7), one can obtain equations corresponding to unit circle and ratio curve as discussed above. As pointed out in the Sect. 4.2.3, $a > b$ (which is the condition for the instability of the first fixed point when $\tau = 0$) is also the condition for the second fixed point to become stable. Correspondingly, the results from the geometric construction reveals that for $\tau > 0$ also the second fixed point attains

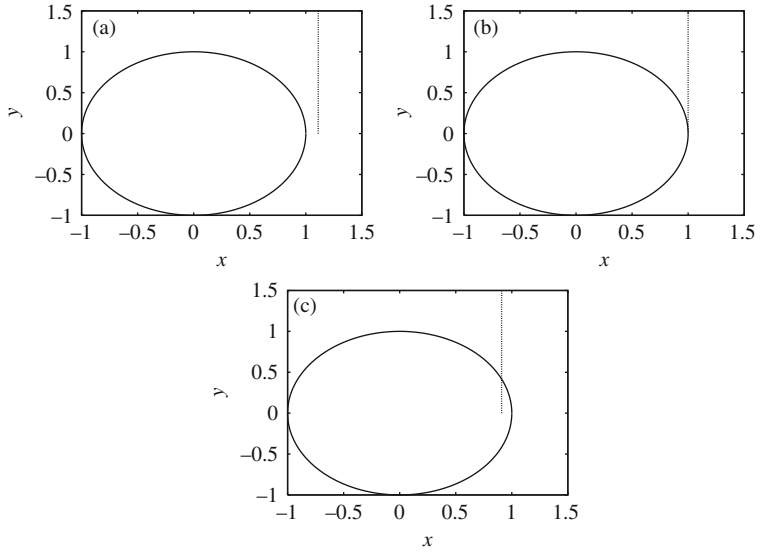

Fig. 4.1 Real and imaginary parts of Eq. (4.7) depicting the change in stability for $\tau = 25.0$ (**a**) For $b = 0.1$, and $a = 0.09$, (**b**) For $b = 0.1$ and $a = 0.1$, and (**c**) For $b = 0.1$ and $a = 0.11$

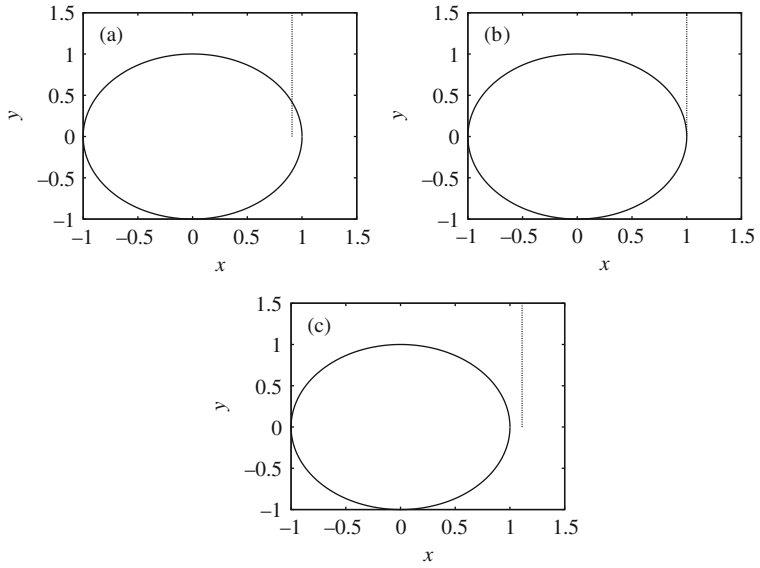

Fig. 4.2 Real and imaginary parts of the characteristic equation corresponding to the second fixed point Eq. (4.2b) at $\lambda = i\beta$ depicting the change in stability for $\tau = 25.0$ (**a**) For $b = 0.1$, and $a = 0.09$, (**b**) For $b = 0.1$ and $a = 0.1$, and (**c**) For $b = 0.1$ and $a = 0.11$

stability when $a > b$ and this is indicated by the intersection of the ratio curve with the unit circle as shown in Fig. 4.2. Here the values of the parameters a, b are kept fixed as in Fig. 4.1 and the value of $c = 10$.

4.2.4.2 General Approach to Determine Stability

Using the general approach discussed in Sect. 2.4 of Chap. 2, we will demonstrate the identification of stable regimes in the (a, τ) parameter space of the fixed point $x^* = 0$ of the Mackey-Glass system (4.1).

Let $\lambda = \alpha + i\beta$ be a root of the transcendental equation (4.6), where α and β are real. Substituting this into the Eq. (4.6) and equating real and imaginary parts, we obtain equations for α and β as

$$\alpha + b - ae^{-\alpha\tau}\cos(\beta\tau) = 0, \tag{4.9}$$

$$\beta + ae^{-\alpha\tau}\sin(\beta\tau) = 0. \tag{4.10}$$

Squaring and adding Eqs. (4.9) and (4.10), we get

$$\beta = \beta_{\pm} = \pm\sqrt{a^2\exp(-2\alpha\tau) - (b+\alpha)^2}, \tag{4.11}$$

and

$$\alpha = -b - \frac{\beta}{\tan(\beta\tau)}. \tag{4.12}$$

Without loss of generality we choose the + sign in the above equation, as the eigenvalues occur in complex conjugate pairs. The change in stability occurs only when the value of α crosses the imaginary axis, $\lambda = i\beta, \beta > 0$, and hence the critical stability curve is the one at which α takes the value $\alpha = 0$. Now, we have

$$\beta|_{\alpha=0} = \pm\sqrt{a^2 - b^2}. \tag{4.13}$$

From Eq. (4.9), it follows that

$$\beta\tau = \pm\arccos\left(\frac{b}{a}\right) + 2n\pi, \tag{4.14}$$

where n is any integer $(0, \pm1, \pm2, \cdots)$. Consequently one can expect that the stability regions are confined between the set of two curves (for $\tau > 0$),

$$\tau_1(n) = \frac{2n\pi + \arccos\left(\frac{b}{a}\right)}{\sqrt{a^2 - b^2}}, \qquad n = 0, 1, 2, \cdots \tag{4.15a}$$

$$\tau_2(n) = \frac{2n\pi - \arccos\left(\frac{b}{a}\right)}{\sqrt{a^2 - b^2}}. \qquad n = 1, 2, 3, \cdots \tag{4.15b}$$

It is to be noted that from Eq. (4.6) when the time-delay $\tau = 0$, $\lambda = -b + a$ and so the real part of λ, $\alpha < 0$ for $b > a$. In order to identify those curves for $\tau > 0$ which encompass the stable regions, the critical curves should be the ones on which $\frac{d\lambda}{d\tau} > 0$. From Eq. (4.6), we have

$$\frac{d\lambda}{d\tau} = \frac{-a\lambda \exp(-\lambda\tau)}{1 + a\tau \exp(-\lambda\tau),} \tag{4.16}$$

and hence

$$\left.\frac{d\alpha}{d\tau}\right|_{\alpha=0} = \frac{\beta^2}{[1 + a\tau\cos(\beta\tau)]^2 + [a\tau \sin(\beta\tau)]^2}. \tag{4.17}$$

Therefore

$$\frac{d\alpha}{d\tau} > 0 \text{ on both } \tau_1 \text{ and } \tau_2. \tag{4.18}$$

The above condition implies that there can be only one stable region (where $\alpha < 0$) between the $\tau = 0$ line and the critical curve $\tau_1(0)$ which is the closest to the line $\tau = 0$ as discussed in Sect. 2.4 and also in Sect. 3.2.1 for the piecewise linear DDE. We note that the condition (4.18) prohibits the existence of any other stable region (that is multistability region) because for a second stable region to exist one requires $\frac{d\alpha}{d\tau} < 0$ on any one of the other curves ($n > 0$). But this never occurs in this case. The numerical plot in Fig. 4.3 of the curves $\tau_1(n)$ (solid curve for $n = 0, 1, 2$) and $\tau_2(n)$ (broken curve for $n = 1, 2$) reveals that the region between $\tau = 0$ and $\tau = \tau_1(0)$ is the only stable region (shaded region), where $\frac{d\alpha}{d\tau} > 0$ on τ_1, which passes from negative to positive values of α. Obviously the other curves $\tau_2(n) < \tau < \tau_1(n)$ for $n > 0$ do not satisfy the required stability condition and hence they are all associated with unstable regions.

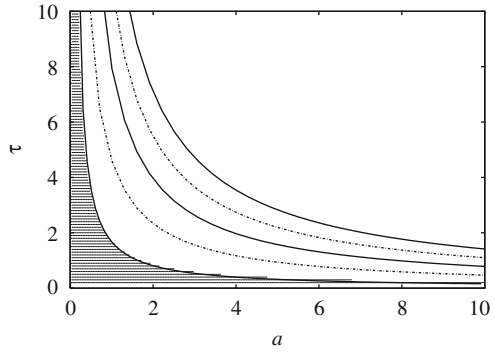

Fig. 4.3 *Curves* of Eqs. (4.15a) and (4.15b). The *solid curves* represent τ_1 for $n = 0, +1, +2$ and *broken curves* represent τ_2 for $n = +1, +2$. The *region* enclosed between the *line* $\tau = 0$ and the *curve* $\tau = \tau_1(0)$ (*shaded region*) is the only stable island of the first fixed point $x^* = 0$ where $\frac{d\alpha}{d\tau} > 0$ on $\tau_1(0)$

One can also perform similar stability analysis using the above approach to identify the stable regimes of the second fixed point $x^* = \left(\frac{a-b}{b}\right)^{\frac{1}{c}}$. Following the procedure used for the fixed point $x^* = 0$, we obtain the set of critical curves corresponding to the characteristic equation (Eq. 4.8) of the second fixed point as

$$\tau_1(n) = \frac{2n\pi + \arccos\left(\frac{b}{k}\right)}{\sqrt{k^2 - b^2}}, \qquad n = 0, 1, 2, \cdots \tag{4.19a}$$

$$\tau_2(n) = \frac{2n\pi - \arccos\left(\frac{b}{k}\right)}{\sqrt{k^2 - b^2}}, \qquad n = 1, 2, 3, \cdots \tag{4.19b}$$

where $k = b(1 - ac + bc)$, along with

$$\left.\frac{d\alpha}{d\tau}\right|_{\alpha=0} = \frac{\beta^2}{[1 + k\tau\cos(\beta\tau)]^2 + [k\tau\sin(\beta\tau)]^2} > 0 \text{ on both } \tau_1 \text{ and } \tau_2. \tag{4.19c}$$

With the same argument as in the previous case of first fixed point, we find that there is only one stable island between the curves $\tau = 0$ and $\tau_1(0)$ as shown in Fig. 4.4.

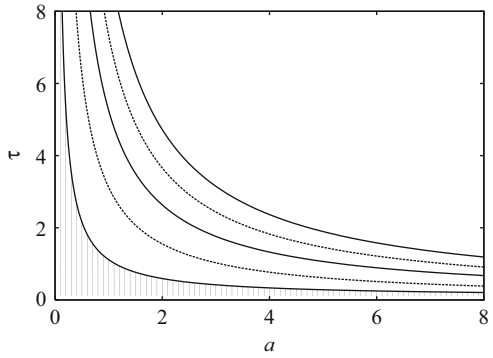

Fig. 4.4 *Curves* of Eqs. (4.19a) and (4.19b). The *solid curves* represent τ_1 for $n = 0, +1, +2$ and *broken curves* represent τ_2 for $n = +1, +2$. The *region* enclosed between the *line* $\tau = 0$ and the *curve* $\tau = \tau_1(0)$ (*shaded region*) is the only stable island of the second fixed point $x^* = \left(\frac{a-b}{b}\right)^{\frac{1}{c}}$ where $\frac{d\alpha}{d\tau} > 0$ on $\tau_1(0)$

4.2.5 Numerical Simulation: Bifurcations and Chaos

In this section, we will briefly discuss the dynamics of the Mackey-Glass time-delay system (4.1) as a function of the delay time τ using numerical simulation. For this purpose, Eq. (4.1) is integrated using Runge-Kutta fourth order integration scheme for the aforesaid parameter values with constant initial condition in

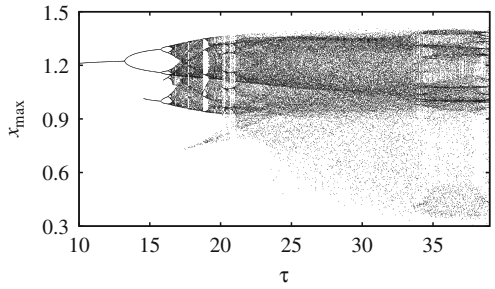

Fig. 4.5 Bifurcation diagram of the Mackey-Glass system (Eq. 4.1) for the parameter values $a = 0.2, b = 0.1, c = 10$ as a function of time-delay $\tau \in (10, 39)$

the range $(-\tau, 0)$ leaving out sufficiently large transients (of the order 1×10^6). For details on the effect of transients, see Chap. 3. Fixing the other parameters as $a = 0.2, b = 0.1$ and $c = 10$, one finds that there is a stable fixed point for $\tau < 4.53$ as we have discussed in the previous section. For $4.53 < \tau < 13.3$, numerical simulations show that there is a stable limit cycle attractor. At $\tau = 13.3$, the period of this limit cycle doubles, initiating a period doubling bifurcation sequence (as shown in Fig. 4.5) that reaches its accumulation point at $\tau = 16.8$. For $\tau > 16.8$ numerical simulations show chaotic attractors at most parameter values, with some limit cycles interspersed in between.

To depict the qualitative nature of the attractors of the Mackey-Glass system, we display a representative portion of the time series in Fig. 4.6 and the corresponding (pseudo) phase plots in Fig. 4.7 by plotting $x(t)$ against $x(t - \tau)$. It is to be noted

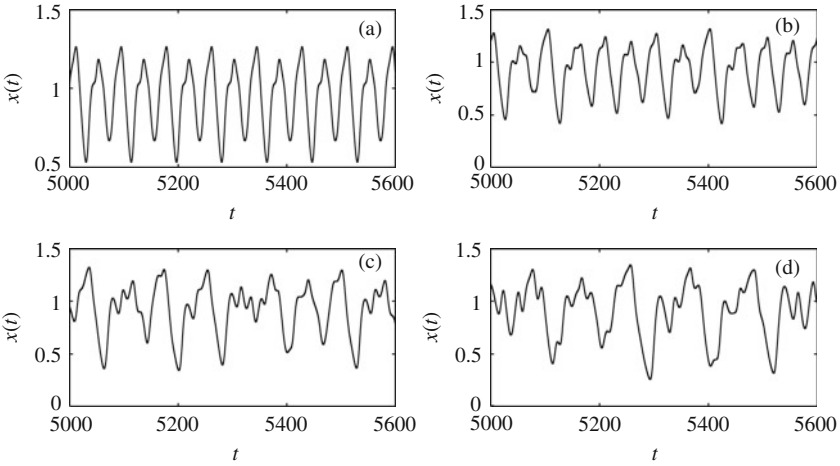

Fig. 4.6 Time series plots of the Mackey-Glass system for the parameter values $a = 0.2$, $b = 0.1, c = 10$ for different values of the delay time τ. (**a**) periodic time trajectory for $\tau = 14$, (**b**) chaotic trajectory at the "onset" for $\tau = 17$, (**c**) chaotic time series for $\tau = 23$ and (**d**) hyperchaotic trajectory for the time-delay $\tau = 32$

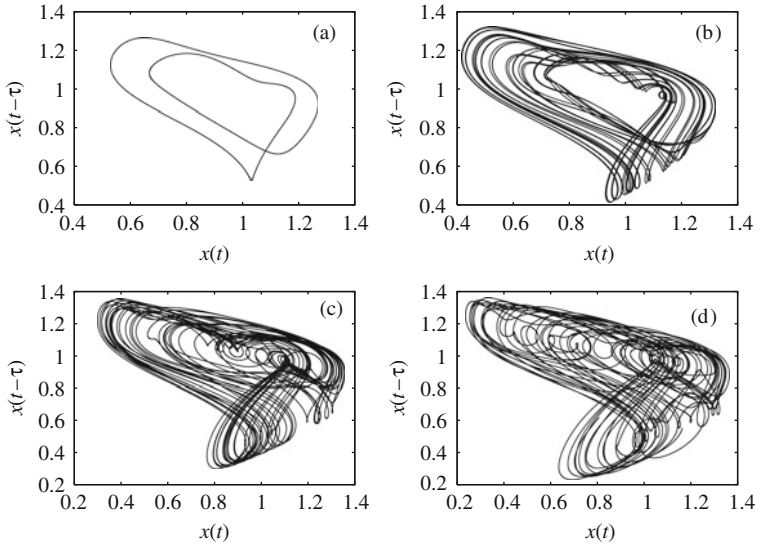

Fig. 4.7 Phase plots obtained by plotting $x(t)$ Vs $x(t-\tau)$ corresponding to the Fig. 4.6

that the choice of $x(t-\tau)$ as the second phase variable is arbitrary; $x(t-t')$ can be equivalently used, where t' is an arbitrary time-delay. A periodic time series is shown in Fig. 4.6a for the delay time $\tau = 14$ and its corresponding phase plot is shown in Fig. 4.7a. Chaotic trajectory at the "onset" of chaos is shown in Fig. 4.6b for the value of delay time $\tau = 17$ along with its phase plot in Fig. 4.7b. Chaotic time series for the value of delay time $\tau = 23$ is shown in Fig. 4.6c with phase plot for the same value of delay in Fig. 4.7c, whereas hyperchaotic trajectory and phase plots are shown in Figs. 4.6d and 4.7d, respectively, for $\tau = 32$.

It may be noted that the above plots (time series and phase plots) are adequate to distinguish periodic behavior from chaotic behavior, but are inadequate to make a sharp distinction between the properties of qualitatively different chaotic behavior and this requires a computation of the corresponding Lyapunov exponents. The first four maximal Lyapunov exponents for the same parameter values as above in the range of delay time $\tau \in (14, 39)$ is shown in Fig. 4.8a. The Lyapunov exponents are evaluated using the procedure suggested by J. D. Farmer [1], described briefly in Sect. 1.2.2. It is clear from the Lyapunov exponents that while the attractors in Fig. 4.7b, c are chaotic, the attractor of Fig. 4.7d is hyperchaotic. The Kaplan-Yorke [1, 20] dimension of the Mackey-Glass system as a function of delay time τ in the same range, obtained by using the formula given in Eq. (3.10), is shown in Fig. 4.8b.

4.2.6 Experimental Realization Using Electronic Circuit

Analog and intrinsic electronic circuits have been employed to mimic the dynamics of Mackey-Glass system [14–17]. Losson et al. [21] have made an attempt in

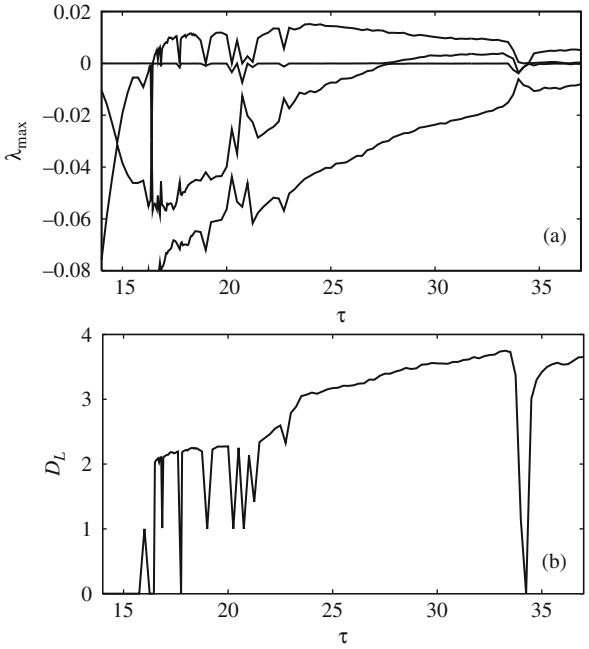

Fig. 4.8 (**a**) Four largest Lyapunov exponents for the same value of parameters as in Fig. 4.6 for the Mackey-Glass system in the range of delay time $\tau \in (14, 39)$ and (**b**) The corresponding Kaplan-Yorke dimension

1993 using analog devices to simulate a delay differential equation; however the nonlinearity used is a piecewise constant model in contrast to the nonlinearity in Mackey-Glass equation, which is a smooth hump shaped nonlinearity as shown in the numerical simulation of the Mackey-Glass nonlinearity in Fig. 4.9a. An electronic analog of the Mackey-Glass system was designed by Namajunas et al. [17] in 1995 and since then this model has been used widely to explore the dynamical and application aspects of the Mackey-Glass system [14–16, 22].

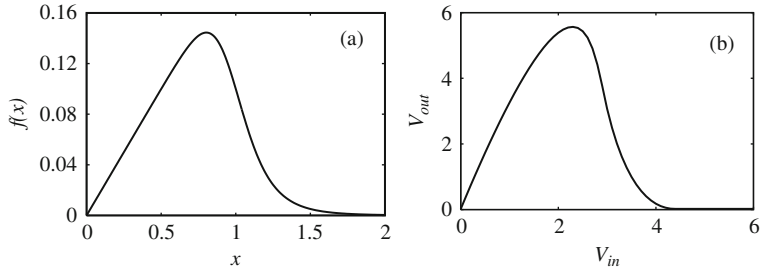

Fig. 4.9 Nonlinearity of the Mackey-Glass system (4.1). (**a**) Plot of the function $f(x) = 0.2x/(1+x^{10})$ obtained by numerical simulation and (**b**) PSPICE simulation of V_{in} Vs V_{out} characteristics of the nonlinear device (Fig. 4.10)

4.2.6.1 Circuit Realization

The block diagram of electronic analog of the Mackey-Glass time-delay system demonstrated in [17] is the same as in Fig. 3.9 shown in Chap. 3. A description of this block diagram is already provided in Sect. 3.4 except for the nonlinearity ND corresponding to the Mackey-Glass system.

A smooth single hump nonlinearity is produced by coupling two complementary junction field-effect transistors (JFETs) [17]. The circuit diagram of nonlinearity is shown in Fig. 4.10. The output voltage from the resistor r is amplified by an operational amplifier (OA) to obtain a sufficient output signal. The output characteristic obtained by PSPICE simulation is shown in Fig. 4.9b. The parameters of the RC filter in Fig. 3.9 are chosen as $R_0 = 3\,\text{KOhm}$, $C_0 = 100\,\text{nF}$, and inductance, capacitance and resistance of the delay unit (Fig. 3.10) as $L = 4.7\,\text{mH}$, $C = 10\,\text{nF}$ (while another possible combination of L and C used widely in the literature is $L = 9.5\,\text{mH}$, $C = 525\,\text{nF}$) and $R = 190\,\text{Ohm}$, respectively. Junction field-effect transistors used in the nonlinear device (Fig. 4.10) are $Q_1 : 2N5457$, $Q_2 : 2N5460$ and $r = 470\,\text{Ohm}$. The PSPICE simulation of the electronic circuit, Fig. 3.9, along with the nonlinearity shown in Fig. 4.10 of the Mackey-Glass system, is shown in Fig. 4.11, which is a quite typical attractor of the Mackey-Glass system (4.1).

Similar electronic circuits have also been considered by Dmitriyev et al. [23]. However they have used a standard delay unit with fixed delay of 64 μs, while RC value is used as a control parameter.

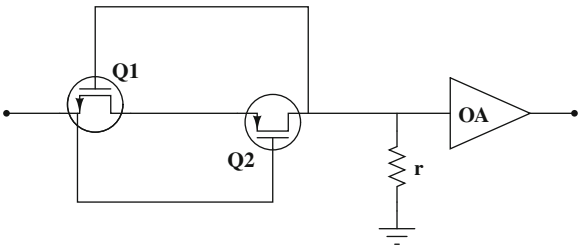

Fig. 4.10 Circuit diagram of the nonlinear device (ND) in Fig. 3.9

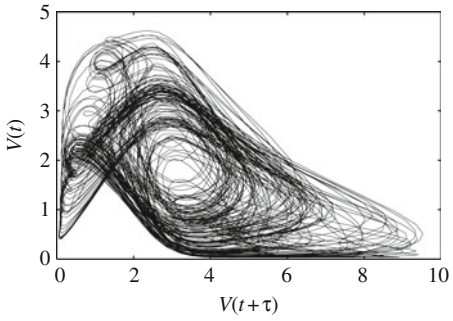

Fig. 4.11 Phase portrait of the analog Mackey-Glass electronic circuit, Fig. 3.9, obtained by PSPICE simulation of the circuit

4.3 Other Interesting Scalar Chaotic Time-Delay Systems

Several simple scalar nonlinear delay systems described by autonomous delay differential equations with suitable nonlinearity have been proposed in the literature in recent times to represent physical and biological systems in view of their potential applications in true random bit generators, global optimization of networks and secure communications, etc. In addition to the piecewise linear and the Mackey-Glass time-delay systems discussed earlier, there are a number of other important scalar chaotic time-delay systems which are being discussed in the literature in the context of chaotic dynamics and chaos synchronization. In this section, we briefly present details of some of them.

4.3.1 A Simple Chaotic Delay Differential Equation

In recent times several attempts have been made to identify simple models that are capable of generating highly complex dynamics for various technological applications. As a consequence, a number of models of delay differential equations and their variants have been proposed and demonstrated in the literature both experimentally and theoretically [24–28] for generating multiple scroll chaotic/hyperchaotic attractors .

In this connection, very recently a simple chaotic delay differential equation has been proposed by J.C. Sprott [26], which can exhibit multiple scroll chaotic/hyperchaotic attractors even for low value of delay time, say $\tau \approx 5$. The delay differential equation is of the form

$$\dot{x} = \sin x(t - \tau). \tag{4.20}$$

Details of stability and bifurcation analysis, and various dynamical behaviors, have been reported in [26]. A 6-scroll hyperchaotic attractor for the value of delay time $\tau = 5.1$ is depicted in Fig. 4.12, while the twelve-largest Lyapunov exponents and the Kaplan-Yorke dimension defined as in Eq. (3.10) in the range of delay time $\tau \in (0, 20)$ are shown in Fig. 4.13a, b, respectively.

4.3.2 Ikeda Time-Delay System

The Ikeda system was introduced to describe the dynamics of an optical bistable resonator and it was shown that the transmitted light from a ring cavity containing a nonlinear dielectric medium undergoes transition from a stationary state to periodic and nonperiodic states, when the intensity of the incident light is increased. It has also been shown that the nonperiodic state is characterized by a chaotic variation of the light intensity and associated broadband noise in the power spectrum [29]. The Ikeda system is well known for delay induced chaotic behavior [30–32] and it is

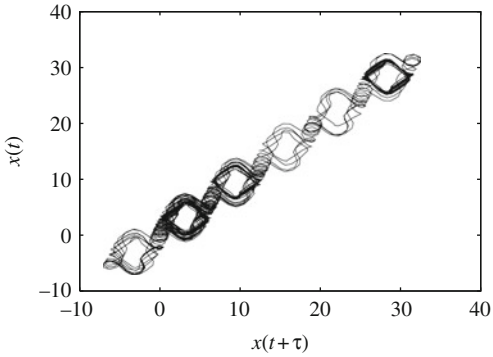

Fig. 4.12 A 6-scroll hyperchaotic attractor of the simple delay differential equation (4.20) for the value of the delay time $\tau = 5.1$

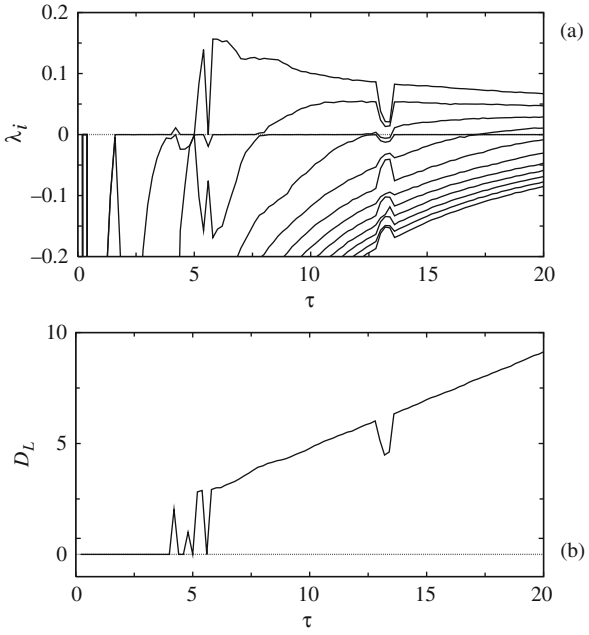

Fig. 4.13 (**a**) Largest twelve Lyapunov exponents and (**b**) Kaplan-Yorke dimension of the simple delay differential equation (4.20) in the range of delay time $\tau \in (0, 20)$

also receiving focus on synchronization studies in recent times [33–36]. The model is specified by the state equation

$$\dot{x} = -\alpha x(t) - \beta \sin x(t - \tau), \tag{4.21}$$

where $\alpha > 0$ and $\beta > 0$ are the parameters and τ is the delay time. Physically $x(t)$ is the phase lag of the electric field across the resonator and thus may clearly assume both positive and negative values, α is the relaxation coefficient, β is the laser intensity injected into the system and τ is the round-trip time of the light in the

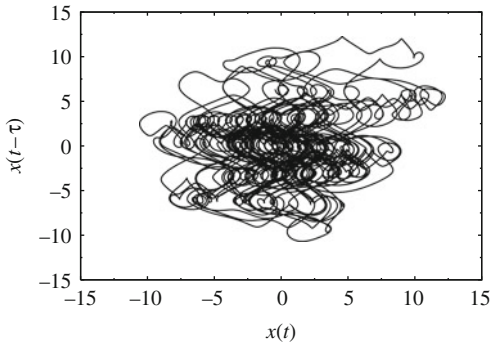

Fig. 4.14 Chaotic attractor of the Ikeda system (4.21) for the values of the parameters $\alpha = 1.0$, $\beta = 20$ and $\tau = 2$

resonator. A typical hyperchaotic attractor of the Ikeda system is shown in Fig. 4.14 for the parameter values $\alpha = 1.0, \beta = 20$ and $\tau = 2$. This system also plays an important role in electronics and physiological studies [33, 35, 37]. Dynamics and associated complexity of the Ikeda model have been discussed in detail in [37]. In particular the dynamics of Ikeda ring cavity laser is explained using an experimental set up and its block diagram along with the emergence of chaos through period-doubling cascade [30–32, 37]. The first eleven maximal Lyapunov exponents of the Ikeda system for the parameters $\alpha = 1.0, \beta = 5$ in the range of delay time $\tau \in (2, 25)$ are shown in Fig. 4.15a and the corresponding Kaplan-Yorke Lyapunov dimension (4.15b) is shown in Fig. 4.15b.

4.3.3 Scalar Time-Delay System with Polynomial Nonlinearity

Recently, Voss [38] introduced a scalar time-delay system with polynomial nonlinearity experimentally in an electronic circuit with the state equation

$$\dot{x} = -\alpha x(t) - f(x(t-\tau)), \tag{4.22}$$

where

$$f(x(t-\tau)) = -10.44x_\tau^3 - 13.95x_\tau^2 - 3.63x_\tau - 0.85, \; x_\tau = x(t-\tau). \tag{4.23}$$

The model has been studied both experimentally and numerically for its chaotic dynamics [38] and real time anticipation of chaotic states has been demonstrated using this circuit. The parameters are chosen such as to closely fit the parameters of the electronic circuit described in [38]. It is also noted that the nonlinearity (4.23) shows a single smooth hump and resembles that of the Mackey-Glass system. The parameter values are fixed as $\alpha = 3.24\,\mathrm{m/s}$ and the delay time $\tau = 13.28\,\mathrm{ms}$ for numerical simulation and for these values the system (4.22) exhibits chaotic dynamics as shown in Fig. 4.16.

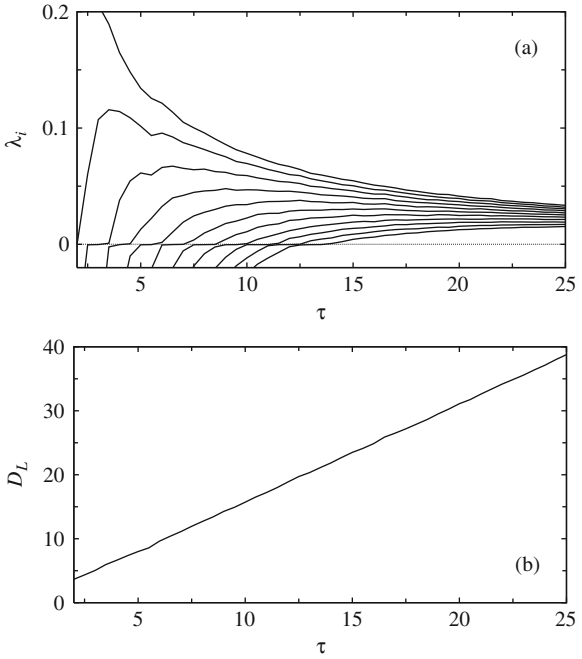

Fig. 4.15 (**a**) Largest eleven Lyapunov exponents of Ikeda system (4.21) for the values of parameters $\alpha = 1.0$, $\beta = 5$ in the range of delay time $\tau \in (2, 25)$ and (**b**) The corresponding Kaplan-Yorke dimension of the Ikeda system

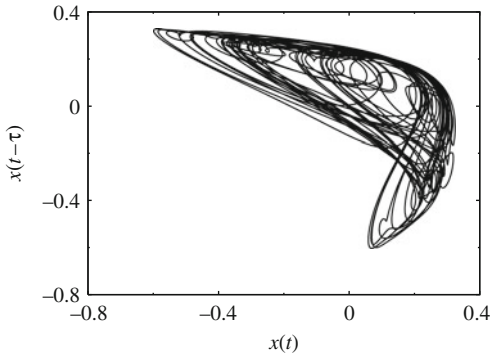

Fig. 4.16 Chaotic attractor of the system (4.22) for the values of the parameters $\alpha = 3.24\,\mathrm{m/s}$ and $\tau = 13.28\,\mathrm{ms}$

4.3.4 Scalar Time-Delay System with Other Piecewise Linear Nonlinearities

In addition to the odd piecewise linear delay differential equation discussed in the previous chapter (Chap. 3), there are several other types of piecewise linear delay differential equations which have been studied in the literature. A delay differen-

tial equation with odd piecewise linear function with only three segments can be defined as

$$\dot{x} = -ax(t) + bf(x(t-\tau)), \tag{4.24}$$

where $f(x)$ is a three segment odd piecewise function represented as

$$f(x) = \begin{cases} d(x+1) - c, & x < -1 \\ cx, & -1 < x < 1 \\ d(x-1) + c, & x > 1, \end{cases} \tag{4.25}$$

System (4.24) and (4.25) has been analyzed in [24, 25] both experimentally and theoretically for the parameter values $c = 2.0$ and $d = -4.0$. The only difference between the three segment odd piecewise linear function and the five segment odd piecewise linear function (2.19) is that nonlinearity does not saturate to zero at larger values of $|x|$. It has been shown that this nonlinearity can generate not only mono-scroll hyperchaotic oscillations but also more complex double-scroll hyperchaotic oscillations for suitable values of delay times. Numerically simulated three segment piecewise linear functional form is depicted in Fig. 4.17a. Mono- and double-scroll

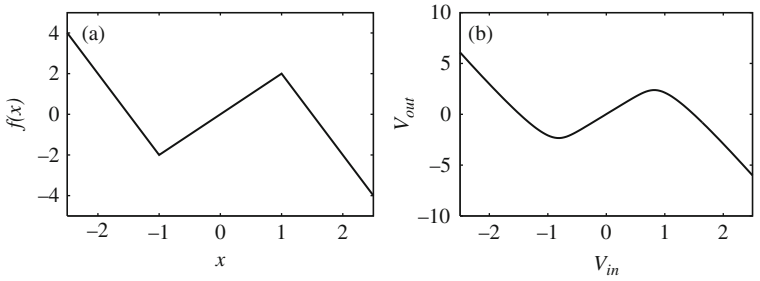

Fig. 4.17 Odd-symmetry nonvanishing three-segment nonlinear function $f(x)$ given by Eq. (4.25) (**a**) Numerical plot and (**b**) PSPICE simulation

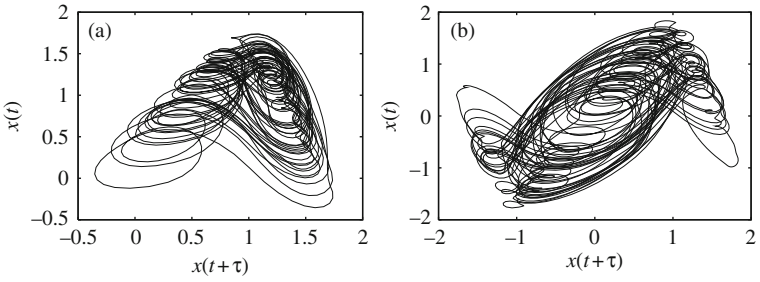

Fig. 4.18 Numerical phase portraits of the systems (4.24) for the values of the parameters $a = 1.0, b = 1.0, c = 2.0$ and $d = -4.0$ (**a**) Mono-scroll attractor for the value of the delay time $\tau = 2.0$ and (**b**) Double-scroll attractor for the value of the delay time $\tau = 8.0$

hyperchaotic attractors for the values of the parameters $a = 1.0, b = 1.0$ and the delay times $\tau = 2.0$ and $\tau = 8.0$ are shown in Fig. 4.18a, b, respectively.

The same block diagram and the delay unit depicted in Figs. 3.9 and 3.10, respectively, can be used to mimic the delay differential equation (4.24) along with the three segment piecewise linear function, Eq. (4.25), by using the nonlinear device (ND) [24, 25] shown in Fig. 4.19. The values of the resistances in the nonlinear device are chosen as $R_1 = R_2 = R_3 = 1\,\text{KOhm}$ and $R_4 = 3\,\text{KOhm}$. Diodes and operational amplifiers in the nonlinear device are chosen as $1N4148$ and $LF356N$, respectively. PSPICE simulation of the output characteristics of the nonlinear device (ND) shown in Fig. 4.19 is depicted in Fig. 4.17b. Mono- and double-scroll hyperchaotic attractors of the circuit (Fig. 3.9) with the nonlinear device (Fig. 4.19) for the corresponding values of the parameters [24, 25] are shown in Fig. 4.20a, b, respectively. Ten largest Lyapunov exponents and the Kaplan-Yorke dimension of the delay differential equation (4.24) with the three segment piecewise linear function in the range of $\tau \in (0, 10)$ for the above values of other parameters are shown in Fig. 4.21.

Other piecewise linear models discussed in the literature include those models where the function $f(x)$ in Eq. (4.24) is of the form

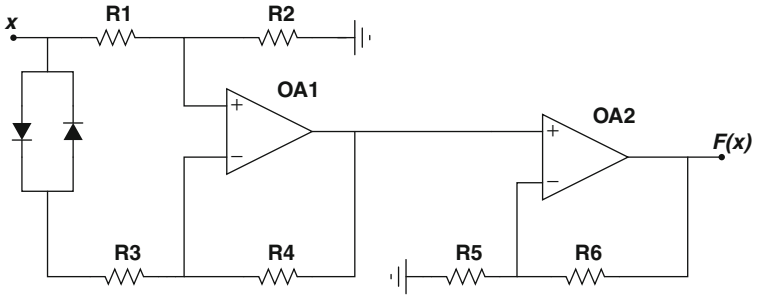

Fig. 4.19 Circuit diagram of the nonlinear device (ND) corresponding to the Eq. (4.25)

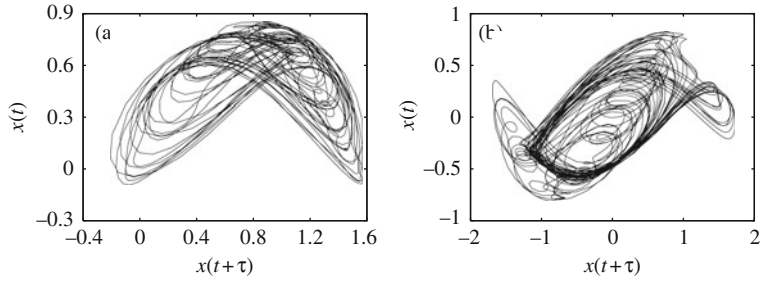

Fig. 4.20 PSPICE simulation of the nonlinear circuit Fig. 4.19 for the corresponding values of the circuit elements (**a**) Mono-scroll attractor and (**b**) Double-scroll attractor

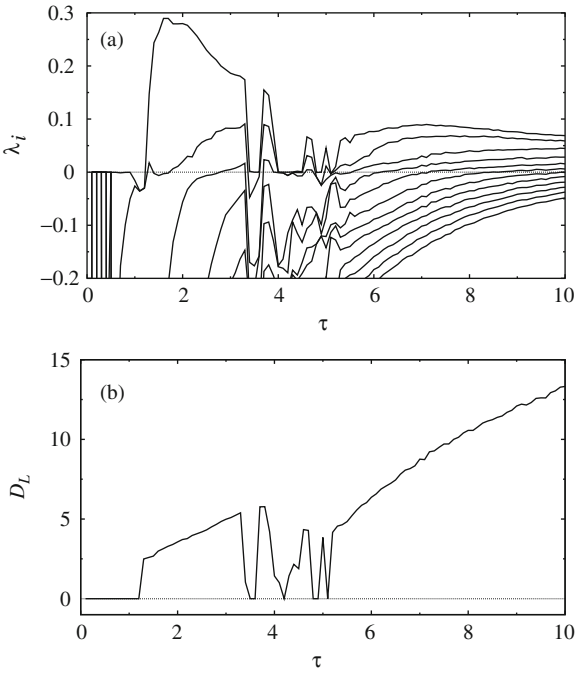

Fig. 4.21 (**a**) Largest twelve Lyapunov exponents and (**b**) Kaplan-Yorke dimension of the piecewise linear delay differential equation (4.24) in the range of delay time $\tau \in (0, 10)$

$$f(x) = \begin{cases} 2x, & x \leq 1/2 \\ 2 - 2x, & x > 1/2, \end{cases} \tag{4.26}$$

and

$$f(x) = \begin{cases} px(1-x), & |x| < 1 \\ 0, & |x| \geq 1. \end{cases} \tag{4.27}$$

These piecewise linear models have been well studied in [11, 21, 39] for their chaotic dynamics and also on synchronization aspects. The chaotic attractor of the system (4.24) with the functional form (4.26) is shown in Fig. 4.22a for the parameter values $\alpha = 0.2$, $\beta = 0.2$ and $\tau = 25$, while the chaotic attractor of the system (4.24) with the piecewise linear function of the form (4.27) for the parameter values $a = 0.2$, $b = 0.2$, $p = 5$ and $\tau = 25$ is shown in Fig. 4.22b.

4.3.5 Another Form of Scalar Time-Delay System

Another form of scalar DDE which has also been used in the literature is

$$\dot{x} = -ax(t-\tau) + bf(x(t-\tau)), \tag{4.28}$$

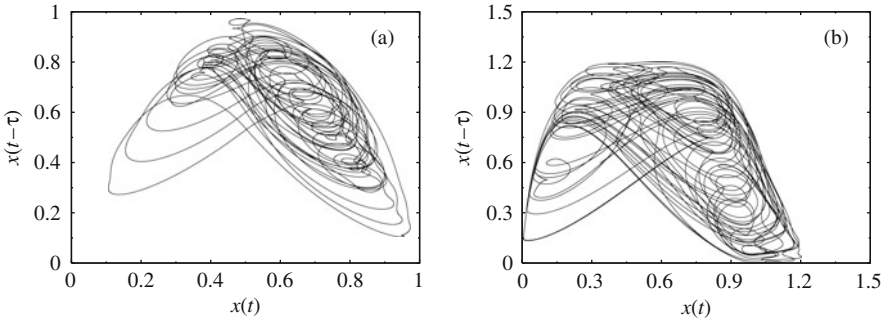

Fig. 4.22 Chaotic attractor of the system (4.24) with (**a**) functional form (4.26) for the values of the parameters $\alpha = 0.2$, $\beta = 0.2$ and $\tau = 25$ and (**b**) piecewise linear function of the form (4.27) for the parameter values $a = 0.2$, $b = 0.2$, $p = 5$ and $\tau = 25$

where a and b are parameters. As a first example to this type of scalar DDE, we will discuss the dynamical system proposed by Yalcin and Ozoguz [28] to generate an n-scroll chaotic attractor. Nonlinearity of this model is based on a hard limiter function and that the model can be easily generalized in a systematic way in order to obtain an n-scroll attractor. The nonlinear function is given by

$$f(x) = \sum_{i=1}^{M} g_{(-2i+1)/2}(x) + \sum_{i=1}^{N} g_{(2i-1)/2}(x) \tag{4.29}$$

and

$$g_\theta(x) = \begin{cases} 1, & x \geq \theta, \theta > 0 \\ 0, & x < \theta, \theta > 0 \\ 0, & x \geq \theta, \theta < 0 \\ 1, & x < \theta, \theta < 0. \end{cases} \tag{4.30}$$

The nonlinearity (4.29) was used for the generalization of the so called Jerk circuit [40]. The set of equilibrium points for the nonlinearity (4.29) with $a = b$ is

$$\Theta_{eq} = \{-M, -M+1, \cdots, N-1, N\}. \tag{4.31}$$

The scrolls are located around the equilibrium points. Therefore the number of scrolls equals the number of equilibrium points. The number of scrolls generated by the nonlinearity (4.29) is equal to $M + N + 1$. Chaotic attractors with three ($M = 1, N = 1$), five ($M = 2, N = 2$), six ($M = 1, N = 4$) and nine ($M = 4, N = 4$) scrolls for the system (4.28) with the nonlinearity (4.29) for the values of the parameters $a = 0.2, b = 0.2$ and $\tau = 20$ are shown in Fig. 4.23a–d, respectively. The above dynamical system (4.28) along with the nonlinearity (4.29) has also been demonstrated using electronic circuits by the same authors.

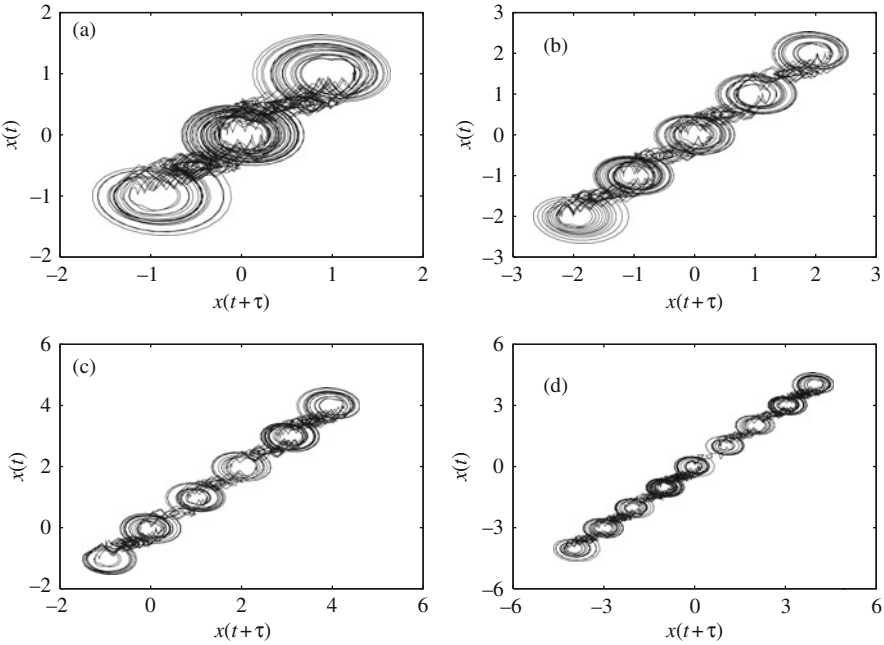

Fig. 4.23 Chaotic attractors of the system (4.28) with nonlinear functional form (4.29) for the values of the parameters $a = 0.2, b = 0.2$ and $\tau = 10$. (**a**) Three-scroll chaotic attractor for $M = N = 1$, (**b**) Five-scroll chaotic attractor for $M = N = 2$, (**c**) Six-scroll chaotic attractor for $M = 1, N = 4$ and (**d**) Nine-scroll chaotic attractor for $M = 4, N = 4$

There are also other types of nonlinear functions used in the literature for the delay differential equation (4.28) with [41]

$$f(x) = sgn(x), \tag{4.32}$$

and

$$f(x) = tanh(10x). \tag{4.33}$$

The chaotic attractors exhibited by the above nonlinearities for the values of the parameters $a = 0.2$, $b = 0.2$ and $\tau = 10$ are depicted in Fig. 4.24a, b, respectively.

Another interesting model with a cubic nonlinear function [26] is,

$$\dot{x} = x(t - \tau) - x^3(t - \tau), \tag{4.34}$$

for which chaos sets in from a limit cycle at $\tau \approx 1.538$. Similar dynamical behavior is also obtained when the signs of both the terms in Eq (4.34) are exchanged. Note that the right hand side of the above equation can be considered as a scaled version of the first two terms in the Taylor series for $\sin(x(t - \tau))$.

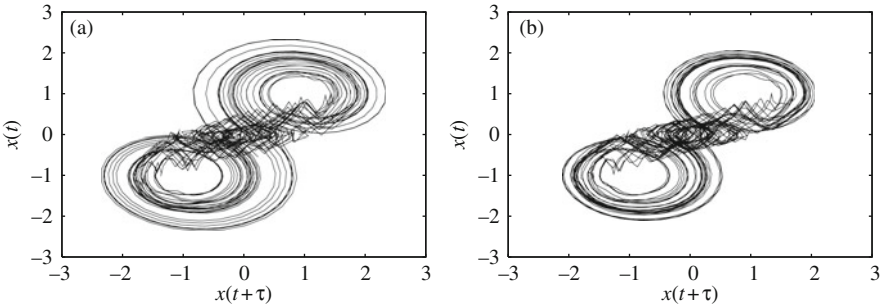

Fig. 4.24 Chaotic attractors of the system (4.28) for the values of the parameters $a = 0.2$, $b = 0.2$ and $\tau = 10$. (**a**) with the nonlinear functional form (4.32) and (**b**) with nonlinear functional form (4.33)

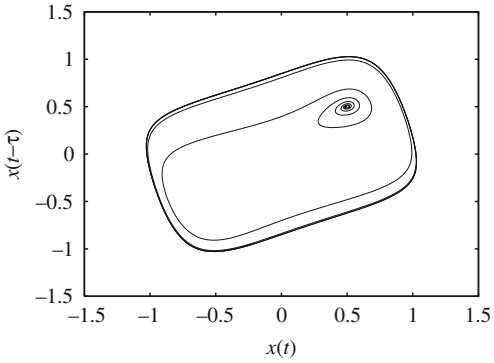

Fig. 4.25 Limit cycle oscillation of the delayed action oscillator (4.35) for the value of the parameters $a = 0.7$, $b = 1$ and delay time $\tau = 2$

4.3.6 El Niño and the Delayed Action Oscillator

A natural atmospheric phenomenon that attracts regular public attention is the El Niño event in the equatorial Pacific. El Niño is an excellent example of the interaction between the ocean and the atmosphere and their combined effect on climate. This phenomenon is a disruption of the ocean-atmosphere system having important consequences for weather around the globe. It results in a redistribution of rains with flooding and droughts. Along the equator, the western Pacific has some of the world's warmest ocean water, while in the eastern Pacific, cool water dwells up, carrying nutrients that support large fish populations. In every two to seven years, strong westward blowing trade wind subsides and warm water slowly moves back eastward across the Pacific, which interrupts the upwelling of cool and nutrient rich water. As a consequence fish die and climatic changes affect many parts of the world.

Historically, the term "El Niño" was used by the fisherman along the west coast of Peru and Ecuador to refer to a warm southward flowing current that moderates the low sea-surface temperature that typically appears around Christmas-time and

therefore named as "El Niño" (the Little Boy or Christ Child in Spanish), which lasts several months. In certain years this current is unusually strong, bringing heavy rains and flooding inland, but also decimating fishing stocks, bird populations, and the other water based wildlife in what would normally be an abundant part of the Pacific.

Today, the term El Niño is most often used when describing a far large-scale warming that can be observed across the whole of the Pacific Ocean by certain characteristic climatic conditions. The effects of El Niño can also be seen globally. Examples include spring rainfall levels in Central Europe, flooding in East Africa, and the ferocity of the hurricane season in the Gulf of Mexico [42]. El Niño is just one phase of the El Niño Southern Oscillation (ENSO) phenomenon, that is, an irregular cycle of coupled ocean temperature and atmospheric pressure oscillations across the whole equatorial Pacific.

El Niño Southern Oscillation phenomenon is a global event arising from large-scale interaction between the ocean and the atmosphere. The Southern Oscillation refers to oscillations in the surface pressure (atmospheric mass) between the south-eastern tropical Pacific and the Australian-Indonesian regions. When the waters of the eastern Pacific are abnormally warm (an El Niño) sea level pressure drops in the eastern Pacific and rises in the west. The reduction in the pressure gradient is accompanied by a weakening of the low-latitude easterly trades.

Usually, coupled atmosphere-ocean general circulation models combined with large scale computing resources are needed to study and predict El Niño's consequences. Fortunately, a route toward qualitative and quantitative prediction based on the *delayed-action oscillator* exists. Recent works on the mechanism of the ENSO have led various simple delay oscillator models which have provided a quite satisfactory explanation for the onset, termination, and cyclic nature of ENSO events, see [43] and references therein. Very recently, a simple model described by a scalar delay differential equation has been shown to mimic most of the observed dynamics of ENSO phenomenon. It models the irregular fluctuations of the sea-surface temperature, and incorporates the full coupled Navier-Stokes dynamics of an El Niño event by a suitably chosen nonlinearity. The corresponding equation can be represented as [42]

$$\dot{x} = kx - bx^3 - ax(t - \tau), \tag{4.35}$$

where k, b, a and τ are constants. The first term on the right-hand side of Eq. (4.35) represents a strong positive feedback within the ocean atmosphere system and the second term is an unspecified nonlinear net damping term that is present to limit the growth of unstable perturbations. The strength of the returning emerging signals relative to that of the local nondelayed feedback is denoted by a.

The delayed oscillator (4.35), as it is, exhibits only limit cycle oscillations (Fig. 4.25). The full model to include every aspect of El Niño event is represented as

$$\dot{x} = kx - bx^3 - ax(t - \tau) + y' + \beta + R(t), \tag{4.36}$$

where $y'(t)$ is the annual cycle which plays an important role in determining the onset of El Niño, β corresponds to global warming which influences the periodicity and amplitude of El Niño events, and $R(t)$ is a stochastic term which influences the irregularity of El Niño events. The full model (4.36) represented by the delayed-action oscillator now mimics the observed richness and variance of the El Niño Southern oscillations phenomenon. Thus the oscillator modeled by delayed feedback serves as an excellent model for observed physical phenomenon. Details of stability analysis and its dynamics can be found in [42].

In addition to the above example of describing a natural phenomenon in terms of delay differential equations/models, recent investigations have also shown that the Neolithic transition (that is, transition from hunter-gatherer to agricultural economy) in Europe has also been successfully described using a time-delay model, which agrees quite well with the observations based on archaeological data. These data led to the conclusion that European farming originated in the Near East, from where it spread across Europe [44].

4.4 Coupled Chaotic Time-Delay Systems

As pointed out in the previous section, a large number of physical, biological, chemical, ecological and economic systems, as well as fluctuations in agricultural commodity prices, neural networks, etc., are successfully modeled by delay differential equations, and thereby capturing many of the inherent complex dynamics of the respective dynamical systems, cf. [4, 18, 21, 41, 45–60]. DDEs are often found not only as scalar first order equations but also as coupled higher order equations. Some of the delay models of chemical, physiological and economic dynamics, mathematical and genetic regulatory systems are represented as coupled higher order DDEs [59, 60]. Rigorous mathematical treatment of such higher order DDEs becomes much more complicated than the case of scalar DDEs and consequently details of such coupled higher order systems are available only through numerical analysis. In the following, we will discuss briefly about some of the important higher order DDEs that have been widely studied in the current literature in the context of chaotic dynamics and chaos synchronization.

4.4.1 Time-Delayed Chua's Circuit

As an example of coupled higher order DDEs in electronic circuits, we present here one of the important second order time-delay systems, namely, time-delayed Chua's circuit (TDCC) which has been realized experimentally using suitable electronic circuit. This was introduced by Sharkovsky et al. [61] and it has been studied in detail by many researchers [62–64]. In particular, the work of Sharkovsky et al. showed that the dimension of state space is increased by substituting the lumped LC resonator with an ideal (lossless) transmission line. TDCC has a constant voltage generator E in series with the Chua's diode as shown in Fig. 4.26 in order to break

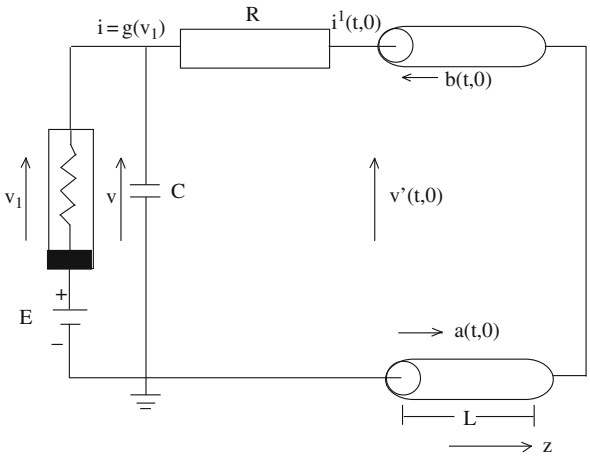

Fig. 4.26 Time-delayed Chua's circuit (TDCC)

the symmetry in the original Chua's diode $v - i$ characteristic. The other elements in the circuit are the lumped linear elements C and $G = 1/R$. The parameters of the circuit are the round trip delay T and the characteristic impedance Z of the transmission line. The line parameters relate to the line per-unit-length inductance l and capacitance c, and they are related to the line length $\mathcal{L}$ as $T = 2\mathcal{L}\sqrt{lc}$ and $Z = \sqrt{l/c}$. The circuit is represented by the coupled normalized equations of the form

$$\theta \dot{x}(t) + \lambda_q(x(t) - E) + q(\lambda_0 - \lambda_q) = (1 - \gamma)(y - 0.5E), \tag{4.37a}$$

$$y(t + 1) = \gamma y(t) - \tfrac{\gamma+1}{2}x(t), \tag{4.37b}$$

where $\lambda_q = \frac{(1-\gamma^2)}{2(\gamma - h_q)}$, $q = -1, 0, 1$, and θ, γ, h_0, h_1, h_{-1} are dimensionless parameters corresponding to the experimental counterparts. Chaotic attractor of the time-delayed Chua's circuit (4.37) for the parameter values $\theta = 0.1616$, $\gamma = -0.58156$, $h_0 = 0.35828$, $h_1 = h_{-1} = -4.9073$ and $E = 0.0$ for the initial conditions $y(\tau) = 0, \tau \in (0, 1)$ is shown in Fig. 4.27.

4.4.2 Semiconductor Lasers

A large number of systems in laser optics have been represented by coupled higher order delay differential equations that are quite complicated than the systems presented in the above sections. Also a large number of papers have appeared in recent times in studying chaos synchronization using laser systems [65–77] as models, in view of the feasibility of experimental realization of high-dimensional chaos.

Now, we will describe a well studied single mode semiconductor laser with optical feedback in the context of chaotic dynamics and its synchronization. All optical feedback in external cavity semiconductor lasers has been a subject of extensive

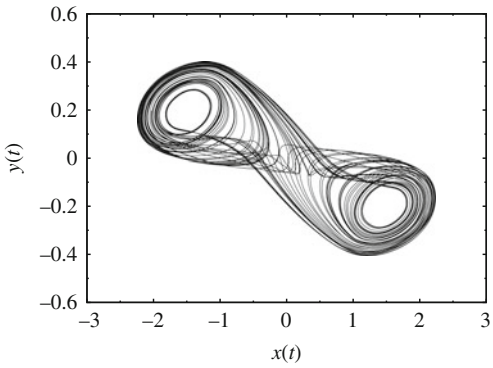

Fig. 4.27 Chaotic attractor of the time-delay Chua's circuit (TDCC) (4.37) for the parameter values $\theta = 0.1616$, $\gamma = -0.58156$, $h_0 = 0.35828$, $h_1 = h_{-1} = -4.9073$ and $E = 0.0$ with initial conditions $y(\tau) = 0, \tau \in (0, 1)$

research during the past decade because of its importance in technical applications such as optical data storage or optical fiber communications [78]. The rate equations for the complex electric fields and the carrier densities in the lasers are the well known Lang-Kobayashi equations [65–67, 71, 74, 75, 79] represented by

$$\dot{E} = \frac{1 + i\alpha}{2}[G(t) - 1/\tau_p]E(t) + \gamma E(t - \tau)\exp[-i(\omega\tau)], \tag{4.38}$$

$$\dot{N} = J/e - N(t)/\tau_n - G(t)|E(t)|^2, \tag{4.39}$$

where E is the slowly varying complex field and N is the normalized carrier number. The equations are written in the reference frame where the complex optical fields of the lasers are given by $E\exp(i\omega t)$, where ω is the optical frequency of the solitary laser [66]. The other parameters are as follows: τ_p is the photon lifetime, α is the line width enhancement factor, $G(t) = G_n(N - N_0)/(1 + \varepsilon|E|^2)$ is the optical gain (where G_n is the differential gain, N_0 is the carrier number at transparency, ε is the gain saturation coefficient), $\omega\tau$ is the phase accumulation after one round trip in the external cavity, τ is the one round trip time of the external cavity, J is the injection current, e is the electric charge, and τ_n is the carrier lifetime. The model does not include multiple reflections in the external cavity, and therefore it is valid for weak feedback levels. For suitable values of the above parameters the laser is in the so-called coherence collapse regime, characterized by fast, chaotic intensity fluctuations. Semiconductor lasers subject to delayed feedback generate chaotic dynamics with intensity pulsations on subnanosecond time scales [78].

Chaos in semiconductor lasers arises in different ways: due to (periodic) modulation of the pump current [80], due to electro-optical feedback where the pump current is modulated by the emitted light intensity [81, 82], or due to an external cavity (optical feedback) [83]. Recently, optoelectronic chaos due to delayed feedback in optoelectronic circuits along with their possible applications has been discussed [84]. All these cases are described by DDEs that exhibit chaotic/hyperchaotic behaviors for suitable values of the parameters. In the above we have provided state equations for semiconductor laser with optical feedback as an example for the coupled higher order DDEs in semiconductor laser systems. It is to be noted that the

semiconductor laser with polarization-rotated optical feedback is described by a 3rd order DDE containing state equations for two complex electric fields E_1 and E_2 with orthogonal polarizations, and a carrier density N [85].

4.4.3 Neural Networks

A class of delayed chaotic neural networks can be represented as the set of coupled DDEs of the form

$$\dot{x}(t) = -Cx(t) + Af\left[x(t)\right] + Bf\left[x(t-\tau)\right], \tag{4.40}$$

where $x(t) = [x_1(t), x_2(t), \cdots, x_n(t)]^T \in R^n$ is the state vector, the activation function $f\left[x(t)\right] = \left(f_1\left[x_1(t)\right], f_2\left[x_2(t)\right], \cdots, f_n\left[x_n(t)\right]\right)^T$ denotes the manner in which the neurons respond to each other. C is a positive diagonal matrix, $A = a_{ij}, i, j = 1, 2, \cdots, n$ is the feedback matrix, $B = b_{ij}$ represents the delayed feedback matrix with a constant delay τ. The general class of delayed neural networks represented by the above Eq. (4.40) unifies several well known neural networks such as the Hopfield neural networks and cellular neural networks with delay.

The delayed neural networks (Eq. 4.40) corresponds to the Hopfield neural networks for the choice of activation function

$$f\left[x(t)\right] = \tanh\left[x(t)\right], \tag{4.41}$$

and for the value of the matrices

$$C = \begin{bmatrix} 1 & 0 \\ 0 & 1 \end{bmatrix}, \; A = \begin{bmatrix} 2.0 & -0.1 \\ -5.0 & 3.0 \end{bmatrix}, \; B = \begin{bmatrix} -1.5 & -0.1 \\ -0.2 & -2.5 \end{bmatrix}.$$

The chaotic behavior of the delayed Hopfield neural network [86, 87] for the above choice of the parameters and for the initial condition $x_0 = [0.1, 0.2]^T$ is shown in Fig. 4.28a. The above general class of delayed neural network represents delayed cellular neural network for the activation function

$$f\left[x(t)\right] = 0.5\left(|x_i + 1| - |x_i - 1|\right), \tag{4.42}$$

and for the value of the matrices

$$C = \begin{bmatrix} 1 & 0 \\ 0 & 1 \end{bmatrix}, \; A = \begin{bmatrix} 1 + \pi/4 & 20 \\ 0.1 & 1 + \pi/4 \end{bmatrix}, \; B = \begin{bmatrix} -\sqrt{2}(\pi/4)1.3 & -0.1 \\ 0.1 & -\sqrt{2}(\pi/4)1.3 \end{bmatrix}.$$

The chaotic attractor of the above delayed cellular neural network for the choice of initial condition $x_0 = [0.1, -0.1]^T$ is shown in Fig. 4.28b.

In the above two sections, we have presented a brief review of some of the important time-delay systems and, in particular, scalar first order time-delay systems with

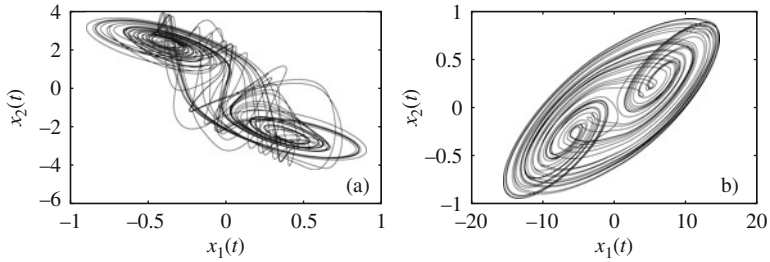

Fig. 4.28 Chaotic behavior of (**a**) Delayed Hopfield neural network and (**b**) delayed cellular neural network

different functional forms for nonlinearity that are widely studied in the literature in the context of chaotic dynamics and chaos synchronization. We have also discussed briefly some of higher order DDEs in different areas. More examples of nonlinear delay systems are given in Appendix D.

References

1. J.D. Farmer, Physica D **4**, 366 (1982)
2. K. Ikeda, M. Matsumoto, J. Stat. Phys. **44**, 955 (1986)
3. M.C. Mackey, L. Glass, Science **197**, 287 (1977)
4. M.C. Mackey, L. Glass, *From Clocks to Chaos, The Rhythms of Life* (Princeton University Press, Princeton, NJ, 1988)
5. W.-H. Kye, M. Choi, M.-W. Kim, S.-Y. Lee, S. Rim, C.-M. Kim, Y.-J. Park, Phys. Lett. A **322**, 338 (2004)
6. M.J. Bunner, M. Popp, Th. Meyer, A. Kittel, J. Parisi, Phys. Rev. E **54**, 3082(R) (1996)
7. C. Zhou, C.H. Lai, Phys. Rev. E **60**, 320 (1999)
8. V.I. Ponomarenko, M.D. Prokhorov, Phys. Rev. E **66**, 026215 (2002)
9. M.D. Prokhorov, V.I. Ponomarenko, Phys. Rev. E **72**, 016210 (2005)
10. W.-H. Kye, M. Choi, S. Rim, M.S. Kurdoglyan, C.-M. Kim, Y.-J. Park, Phys. Rev. E **69**, 055202(R) (2004)
11. I.G. Szendro, J.M. Lopez, Phys. Rev. E **71**, 055203 (2005)
12. K. Pyragas, Phys. Rev. E **58**, 3067 (1998)
13. M. Zhan, X. Wang, X. Gong, G.W. Wei, C.H. Lai, Phys. Rev. E **68**, 036208 (2003)
14. M.-Y. Kim, C. Sramek, A. Uchida, R. Roy, Phys. Rev. E **74**, 016211 (2006)
15. A. Kittle, J. Parisi, K. Pyragas, Physica D **112**, 459 (1998)
16. S. Sano, A. Uchida, S. Yoshimori, R. Roy, Phys. Rev. E **75**, 016207 (2007)
17. A. Namajunas, K. Pyragas, A. Tamasevicius, Phys. Lett. A **201**, 42 (1995)
18. R. Bellman, K.L. Cooke, *Differential-Difference Equations* (Academic Press, New York, 1963)
19. N. McDonald, *Biological Delay Systems: Linear Stability Theory* (Cambridge University Press, Cambridge, 1989)
20. J. Kaplan, J. Yorke, in *Functional Differential Equations and Approximation of Fixed Points*, ed. by H.O. Peitgen, H.O. Walther. Lecture Notes in Mathematics, vol 730 (Springer, Berlin, 1979)
21. J. Losson, M.C. Mackey, A. Longtin, Chaos **3**, 167 (1993)
22. W. Horbelt, J. Timmer, H.U. Voss, Phys. Lett. A **299**, 513 (2002)
23. A.S. Dmitriyev, Yu.N. Orlov, S.O. Starkov, Radiotekh. Elektron **34**, 1980 (1989)

24. A. Tamasevicius, G. Mykolaitis, S. Bumeliene, Electron. Lett. **42**, 13 (2006)
25. A. Tamasevicius, T. Pyragiene, M. Meskauskas, Int. J. Bifurcat. Chaos **17**, 3455 (2007)
26. J.C. Sprott, Phys. Lett. A **366**, 397 (2007)
27. L. Wang, X. Yang, Electron. Lett. **42**, 1439 (2006)
28. M.E. Yalcin, S. Ozoguz, Chaos **17**, 033112 (2007)
29. K. Ikeda, H. Daido, O. Akimoto, Phys. Rev. Lett. **45**, 709 (1980)
30. K. Ikeda, K. Matsumoto, Physica D **29**, 223 (1987)
31. C. Masoller, D.H. Zanette, Physica A **300**, 359 (2001)
32. M. Le Berre, E. Ressayre, A. Tallet, H.M. Gibbs, D.L. Kaplan, M.H. Rose, Phys. Rev. A **35**, 3020 (1987)
33. H.U. Voss, Phys. Rev. E **61**, 5115 (2000)
34. E.M. Shahverdiev, S. Sivaprakasam, K.A. Shore, Phys. Rev. E **66**, 017204 (2002)
35. E.M. Shahverdiev, S. Sivaprakasam, K.A. Shore, Phys. Lett. A **292**, 320 (2002)
36. E.M. Shahverdiev, K.A. Shore, Phys. Rev. E **71**, 016201 (2005)
37. L. Larger, J.P. Goedgebuer, V. Udaltsov, C. R. Physique **5**, 669 (2004)
38. H.U. Voss, Int. J. Bifurcat. Chaos **12**, 1619 (2002)
39. Y.C. Tian, F. Gao, Physica D **108**, 113 (1997)
40. M.E. Yalcin, S. Ozoguz, J.A.K. Suykens, J. Vandewalle, Int. J. Bifurcat. Chaos **12**, 23 (2002)
41. R.D. Driver, *Ordinary and Delay Differential Equations* (Springer, New York, 1977)
42. I. Boutle, R.H.S. Taylor, R.A. Romer, Am. J. Phys. **75**, 15 (2007)
43. E. Tziperman, M.A. Cane, S.E. Zebiak, J. Atmos. Sci. **52**, 293 (1995)
44. J. Fort, V. Mendez, Phys. Rev. Lett. **82**, 867 (1999)
45. J.K. Hale, *Theory of Functional Differential Equations* (Springer, New York, 1977)
46. D.V. Ramana Reddy, Ph. D. Thesis entitled *Collective Dynamics of Delay Coupled Oscillators* (Institute for Plasma Research, Gandhinagar, India, 2000)
47. I. Gyori, P. Ladas, *Oscillation Theory of Delay Differential Equations: With Applications* (Clarendon Press, Oxford, 1991)
48. R. Ross, *The Prevention of Malaria* (John Murray, London, 1911)
49. P.K. Asea, P.J. Zak, J. Econ. Dyn. Control **23**, 1155 (1999)
50. M. Kalecki, Econometrica **3**, 327 (1935)
51. Y. Kuang, *Delay Differential Equations with Applications in Population Dynamics* (Academic Press, Boston, MA, 1993)
52. V. Volterra, *Lecons sur la theorie mathematique de la lutte pour la vieynamics* (Gauthiers-Villars, Paris, 1931)
53. N. MacDonald, *Time Lags in Biological Models*. Lectuer Notes in Biomathematics (Springer, Berlin, 1978)
54. R.M. May, *Stability and Complexity in Model Ecosystems* (Princeton University Press, Princeton, NJ, 1974)
55. K. Gopalsamy, *Stability and Oscillations in Delay Differential Equations of Population Dynamics* (Kluwer Academic Publishers, Dordrecht, 1992)
56. A.D. Drozdov, V.B. Kolmanovskii, *Stability in Viscoelasiticity* (North-Holland, Amsterdam, 1994)
57. J.M. Cushing, *Integrodifferential Equations and Delay Models in Population Dynamics*. Lectuer Notes in Biomathematics, vol. 20 (Springer, Berlin, 1977)
58. J.K. Hale, S.M. Verduyn Lunel, *Introduction to Functional Differential Equations* (Springer, New York, 1993)
59. K. Sriram, Ph. D. thesis on *Modelling Nonlinear Dynamics of Chemical and Circadian Rhythms Using Delay Differential Equations* (Department of Chemistry, IIT, Madras, India, 2004)
60. Alwyn Scott (ed.), *Encyclopedia of Nonlinear Science* (Routledge, New York, 2005)
61. A.N. Sharkovsky, Y. Maisternko, P. Deregel, L.O. Chua, J. Circuits Syst. Comput. **3**, 645 (1993)
62. M. Biey, B.F. Gilli, I. Maio, IEEE Trans. Circuits Syst. I **44**, 486 (1997)

63. M. Gilli, G.M. Maggio, IEEE Trans. Circuits Syst. I **43**, 827 (1996)
64. P. Thangavel, K. Murali, D.V. Senthilkumar, M. Lakshmanan, Int. J. Bifurcat. Chaos (Submitted)
65. C. Masoller, Phys. Rev. Lett. **86**, 2782 (2001)
66. A. Locquet, C. Masoller, C.R. Mirasso, Phys. Rev. E **65**, 056205 (2002)
67. E.M. Shahverdiev, S. Sivaprakasam, K.A. Shore, Phys. Rev. E **66**, 037202 (2002)
68. S. Sivaprakasam, E.M. Shahverdiev, K.A. Shore, Phys. Rev. Lett. **87**, 154101 (2001)
69. S. Sivaprakasam, I. Pierce, P. Rees, P.S. Spencer, K.A. Shore, Phys. Rev. A **64**, 013805 (2001)
70. S. Tang, J.M. Liu, Phys. Rev. Lett. **90**, 194101 (2003)
71. I. Wedekind, U. Parlitz, Phys. Rev. E **66**, 026218 (2002)
72. L.B. Shaw, I.B. Schwartz, E.A. Rogers, R. Roy, Chaos **16**, 015111 (2006)
73. A. Murakami, Phys. Rev. E **65**, 056617 (2002)
74. E.M. Shahverdiev, S. Sivaprakasam, K.A. Shore, Phys. Rev. E **66**, 017206 (2002)
75. J. Ohtsubo, IEEE J. Quantum Electron. **38**, 1141 (2002)
76. L. Wu, S. Zhu, Phys. Lett. A **315**, 101 (2003)
77. A.S. Landsman, I.B. Schwartz, Phys. Rev. E **75**, 026201 (2007)
78. I. Fischer, G.H.M. van Tartwijk, A.M. Levine, W. Elsaesser, E. Goebel, D. Lenstra, Phys. Rev. Lett. **76**, 220 (1996)
79. R. Lang, K. Kobayashi, IEEE J. Quantum Electron. **QE-16**, 347 (1980)
80. J. Sacher, D. Baums, P. Panknin, W. Elsaesser, E.O. Goebel, Phys. Rev. A **45**, 1893 (1992)
81. C.-H. Lee, S.-Y. Shin, Appl. Phys. Lett. **62**, 922 (1993)
82. S.I. Turovets, J. Dellunde, K.A. Shore, J. Opt. Soc. Am. B **14**, 200 (1997)
83. J. Mork, B. Tromborg, J. Mark, IEEE J. Quantum Electron. **28**, 93 (1992)
84. L. Larger, J.M. Dudley, Nature **465**, 41 (2010)
85. D.W. Sukow, A. Gavrielides, T. McLachlan, G. Burner, J. Amonette, J. Miller, Phys. Rev. A **74**, 023812 (2006)
86. J. Meng, X. Wang, Chaos **17**, 023113 (2007)
87. H. Zhu, B. Cui, Chaos **17**, 043122 (2007)